



# Experimental study on the shear characteristics and weakening mechanism of water-bearing rock joints

Weinan Wang<sup>1,2</sup> · Qiangling Yao<sup>1,2</sup> · Chuanjin Tang<sup>3</sup> · Xuehua Li<sup>1,2</sup> · Zhaohui Chong<sup>1,2</sup> · Qiang Xu<sup>1,2</sup>

Received: 9 March 2021 / Accepted: 27 July 2021 / Published online: 2 August 2021  
© Springer-Verlag GmbH Germany, part of Springer Nature 2021

## Abstract

To study the weakening mechanism of the shear characteristics of water-bearing rock joints, four types of artificial saw-tooth joints (including tooth inclination angles of 0°, 15°, 30° and 45°) were prepared in sandstone with four moisture content (0%, 1.55%, 3.1% and 4.65%). This work adopted the non-destructive water intrusion, X-ray diffraction (XRD), acoustic emission (AE) and direct shear tests to mainly investigate the water and inclination angle-induced changes in shear mechanical properties, failure modes and AE characteristics of sandstone rock joints. The results show that the sandstone specimens contain quartz (91.04%), kaolinite, illite and montmorillonite, among which the content of quartz decrease while that of kaolinite and illite increase under the action of water, except that montmorillonite is a little controversial. The shear failure modes of the tested rock joints are divided into climbing, climbing-gnawing combined and gnawing. The inclination angle, followed by normal stress, has the greatest effect on the shear failure modes, and the moisture content has the least effect by comparison. The cohesion and internal friction angle have a positive linear relationship with the inclination angle and a negative linear relationship with the moisture content. According to the test results and Mohr–Coulomb model, a shear strength calculation model of rock joints considering the effect of inclination angle and moisture content is established. The intensity of the AE signal released during specimen failure increases with increasing inclination angle and decreases with moisture content.

**Keywords** Direct shear test · Rock joint · Moisture content · Acoustic emission · Mohr–Coulomb model

## Introduction

Rock masses are discontinuous and complex geological bodies composed of rock blocks and rock joints (Liu and Liu 2017). The stability of rock masses depends on the properties of the intact rocks and the rock joints (Gu et al. 2017) because the shear strength of rock joints is lower than that of intact rocks. Therefore, rock masses with joints are more prone to shear failure under loading than intact rocks (Kulatilake et al. 2001).

Common rock mass instabilities caused by rock joint failure in engineering practice include reservoir dam bedrock landslides, slope instability landslides, rock joint sliding rockbursts and fault sliding earthquakes (Cabrera et al. 2015; Jia and Zhu 2012; Kostic 2017; Tada et al. 2002).

The importance of rock joints to engineering rock masses makes them an important scientific problem in the field of rock mechanics. The most direct method to study the influence factors of rock joint strength (e.g., normal stress, shear direction, rock joint type, etc.) is to conduct laboratory direct shear experiments on regular saw-tooth rock joints (Indraratna and Haque 1997; Bahaaddini 2017) or certain roughness rock joints (Lee et al. 2001). Furthermore, Kou et al. (2019) studied the damage characteristics of sandstone joints with subordinate asperities and they analysed the effects of rate, amplitude and cyclic loading times. Acoustic emission (AE) is a phenomenon associated with the rock failure process and plays an important role in the study of rock fracture (Lockner 1993), by which researchers obtained the special AE parameters (including count, energy, failure location, etc.) and derived parameters (the *b* value in Gutenberg-Richter law) of the rock joints under

✉ Qiangling Yao  
yaoqiangling@cumt.edu.cn

✉ Chuanjin Tang  
chuanjin.tang@nottingham.ac.uk

<sup>1</sup> Key Laboratory of Deep Coal Resource Mining, Ministry of Education, China University of Mining and Technology, Xuzhou 221116, China

<sup>2</sup> School of Mines, China University of Mining and Technology, Xuzhou 221116, China

<sup>3</sup> Department of Civil Engineering, University of Nottingham, Nottingham NG7 2RD, UK

the action of different factors in direct shear experiments (Li et al. 2015; Zhou et al. 2016; Meng et al. 2016). In terms of the theoretical study of rock joint strength, Patton (1966) was the first to put forward the shear strength calculation formula of rock joints, and then, Ladanyi and Archambault (1970) improved the Patton formula and established the Ladanyi shear strength calculation model. After that, the Barton model (Barton and Choubey 1977), Plesha model (Plesha 1987) and Amadei-Saeb model (Saeb and Amadei 1992) were proposed. These theories are constantly improved and developed.

Although many studies have been performed on the shear strength and deformation characteristics of rock joints, most of these studies did not consider the effect of water. In engineering practice, water and rock joints are the key factors controlling the rock damage pattern by markedly changing the mechanical properties (Zhou et al. 2018), thus the effect of water on rock joints cannot be ignored. For example, rainfall is the main factor inducing landslides (Marc et al. 2018), and water intrusion easily causes dam foundation instability (Clarkson and Williams 2021). Yao et al. (2016), Kalachev et al. (2018), and Maruvanchery and Kim (2019) have performed a considerable amount of research on the weakening of rock mechanical properties by water, highlighting the importance of water–rock interactions in geotechnical engineering. Figure 1 illustrates the effect of water on rock joints. The adhesion of water molecules will form a water film on the joint surface and reduce the friction coefficient between the corresponding rock blocks. Furthermore, when water enters the rock joint, the mechanical properties of the rock joint will gradually weaken due to complex effects of water–rock interactions. Wang et al. (2019) studied the influence of water on the joint morphological parameters ( $S_q$ ,  $S_s$  and  $S_k$ ) and fractal dimension through three-dimensional scanning, finding that water increased the roughness of the joint surface. Yang et al. (2019) found that the joint thickness accelerated P-wave attenuation while water restrained P-wave attenuation. Tang et al. (2019b) conducted saturation and direct shear experiments on joint samples made by tension splitting and discovered the different weakening effects

of water under the action of high and low normal loads. To improve the stress environment of jointed rock mass, the method of grouting (Salimian et al. 2017) or grouted bolt (Deb and Das 2014) is usually adopted in engineering. Therefore, it is necessary to study the shear characteristics and shear strength weakening mechanism of water-bearing rock joints, considering the importance of water to the mechanical properties of rock joints and engineering design and relatively few studies of water on rock joints.

In this work, taking the regular saw-tooth sandstone joints with different tooth inclination angles and water content as the research objects, the water absorption law, mineral composition change, and the shear mechanics characteristics and AE characteristics of the samples in direct shear tests were studied, according to which a shear strength formula of the rock joints considering the influence of inclination angle and water content was established. The research results can provide references for the related rock mechanics tests and the engineering researches on the deformation and failure mechanism of water-bearing rock.

## Experimental scheme

### Specimen preparation

The sandstone samples were taken from a rock slope in Renshou County, Meishan city, Sichuan Province, China, and were processed into 50-mm side length of cube specimens with four types of saw-tooth rock joints (including tooth inclination angles of  $0^\circ$ ,  $15^\circ$ ,  $30^\circ$  and  $45^\circ$ ). The length of the saw teeth along the rock joints was 10 mm (Fig. 2). Except for the  $0^\circ$  rock joints, there were five saw teeth on each rock joint.

A total of 171 rock joint specimens were prepared, of which 3 specimens were tested for water intrusion law at the beginning, 144 specimens were tested in direct shear tests and the remaining 24 specimens were made spare. The effective specimens were divided into 48 groups with 3 specimens

**Fig. 1** Effect of water on a rock joint

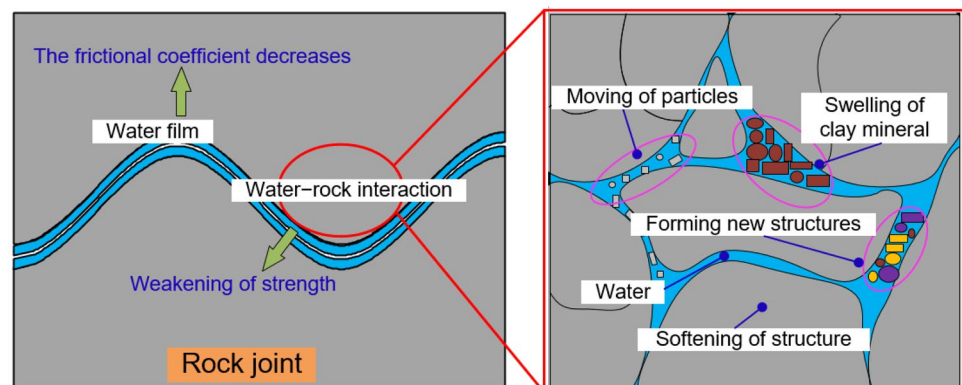
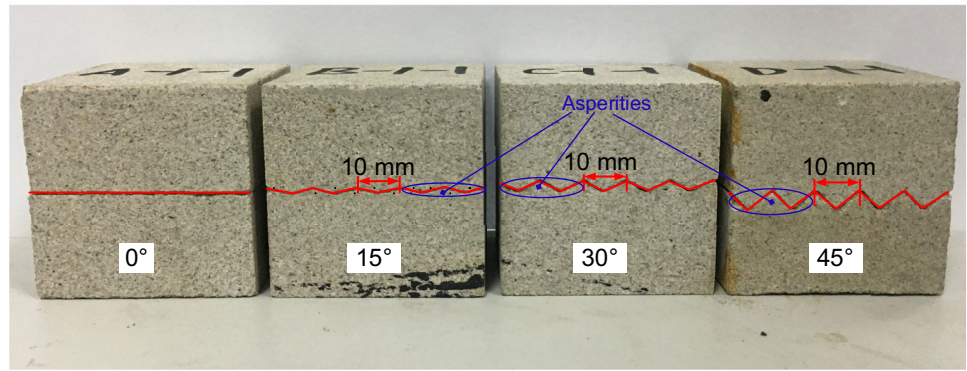


**Fig. 2** Sandstone specimens with saw-tooth joints



in each group according to four inclination angles, four moisture content and three normal stresses. If the test failed, the spare specimens were tested as a supplement. The rock joint specimens were labelled in the scheme of “inclination angle-moisture content-normal stress-specimen number”, as shown in Table 1. For example, A-1-2-3 refers to the third specimen with an inclination angle of 0° and moisture content of 0 for a direct shear test under a 4-MPa normal stress, and B-2-3-1 refers to the first specimen with an inclination angle of 15° and moisture content of 1.55% for a direct shear test under a 5-MPa normal stress.

**Experimental equipment and methods**

The test equipment included a thermostatic drier (101-2, Shanghai Laboratory Instrument Works, China), an automatic non-destructive water intrusion experimental device (ANDWID), an X-ray diffractometer (D8 ADVANCE, Bruker, Germany), a microcomputer-controlled electronic universal testing machine (WDW-300, Jinan Fangyuan Testing Instrument Co., Ltd., China), a self-developed hydraulic normal stress loading system, and an AE monitoring system (PCI-2, Physical Acoustics, USA).

The ANDWID, as shown in Fig. 4a, consists of an ultrasonic humidifier, a sealable box, high-precision loading cells, a data recording and transmission system and a water pump system. The water intrusion principle of ANDWID is that water mist created by the ultrasonic humidifier enters

the sealable specimen box through the plastic hose and produces a high-moisture environment. Using this method, specimens gradually reach saturation state while keeping intact during the intrusion process (Yao et al. 2016; Tang et al. 2019a). The ANDWID can automatically monitor the specimen mass by the high-precision loading cells and recycle the water in the ANDWID by the water pump system at the bottom of the sealable box.

During water immersion, the ANDWID recorded the sample mass per minute. Before and after water immersion, the XRD tests were performed on the dry and wet powder samples (with a particle size less than 38 μm), respectively, to acquire mineral composition and content. The formula for calculating the specimen moisture content is as follows:

$$\omega_a = (m_w - m_d) / m_d \times 100\% \tag{1}$$

where  $\omega_a$  is the moisture content;  $m_w$  is the mass of wet specimen, g; and  $m_d$  is the mass of dry specimen, g.

Schematic diagrams of the loading and AE systems are shown in Fig. 3b. The microcomputer-controlled electronic universal testing machine applied shear stress and the self-developed hydraulic mechanical device applied normal stress. The self-developed hydraulic mechanical device is equipped with a 120-mm stroke of telescopic hydraulic cylinder, a 1.5 kW rated power of automatic control electric hydraulic motor, a high-precision hydraulic gauge and a regulating valve. The sampling frequency of the AE monitoring

**Table 1** Labelling scheme

| Tag (1st letter)        | A              | B              | C          | D              |
|-------------------------|----------------|----------------|------------|----------------|
| Inclination angle/°     | 0              | 15             | 30         | 45             |
| <b>Tag (1st number)</b> | <b>A-1</b>     | <b>A-2</b>     | <b>A-3</b> | <b>A-4</b>     |
| Moisture content/%      | 0              | 1.55           | 3.1        | 4.65           |
| <b>Tag (2nd number)</b> | <b>A-1-1</b>   | <b>A-1-2</b>   |            | <b>A-1-3</b>   |
| Normal stress /MPa      | 3              | 4              | 5          |                |
| <b>Tag (3rd number)</b> | <b>A-1-1-1</b> | <b>A-1-1-2</b> |            | <b>A-1-1-3</b> |
| Specimen number         | First          | Second         |            | Third          |

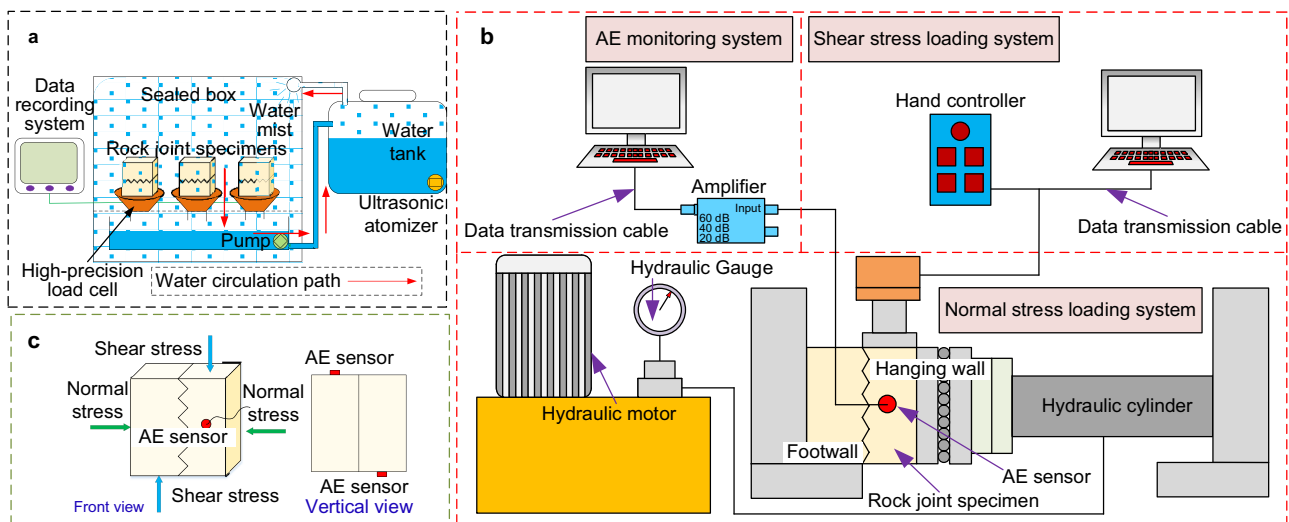


**Fig. 3** Test system. **a** Schematic diagram of the ANDWID (simplified from Tang et al. 2021). **b** Schematic diagram of the loading systems. **c** Sample load

system was 20 Hz. Two AE sensors were used with a gain of 40 dB, resonant frequency of 55 kHz, threshold value of 45 dB and operating frequency range of 35 to 100 kHz. To ensure the synchronous acquisition of the shear stress and AE data during tests, the sampling intervals of the electronic universal testing machine and AE monitoring system were both set to 1  $\mu$ s.

The rock joint specimen was put in place, and the hydraulic mechanical device was then opened to slowly elongate the hydraulic cylinder to apply normal stress on the specimen. The specimen side in contact with the press ram of hydraulic mechanical device was defined as the hanging

wall, and the other side was the footwall. The three normal stresses investigated in the direct shear tests were 3, 4 and 5 MPa. Then, the electronic universal testing machine started to apply the shear stress to the rock joint specimen with a 0.5 mm/min of loading rate. Additionally, the shear stress was along the elevation direction and the normal stress was along the horizontal direction. Because the shear stress applied was much greater than the specimen gravity, the influence of specimen gravity can be ignored.

## Results and discussion

### Water intrusion law of rock specimens

The evolution of the average moisture content of three specimens with intrusion time is shown in Fig. 4. The moisture content changes exponentially with water intrusion time, showing an upward trend of decreasing increase rate. In the first 384 min (rapidly rising stage), the moisture content increases almost linearly from 0 to 4.02% with an average increase rate of 0.01%/min. From 384 to 4000 min (slowly rising stage), the curve slope begins to decrease, that is, the moisture content increase rate is going to decrease. After 4000 min (stable stage), the curve is approximately parallel to the time axis because the moisture content hardly increases; thus, the specimens are considered to be saturated (4.65%). Finally, the representative moisture contents selected for the direct shear tests are 0 (dry), 1.55%, 3.1% and 4.65% (saturated) with the same interval, and the moisture content-water intrusion time curve provides the reference times for the water intrusion tests.

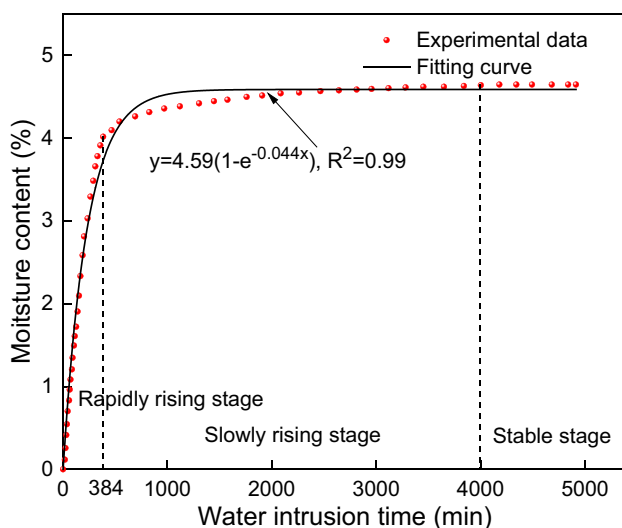


**Fig. 4** Variations in moisture content with intrusion time



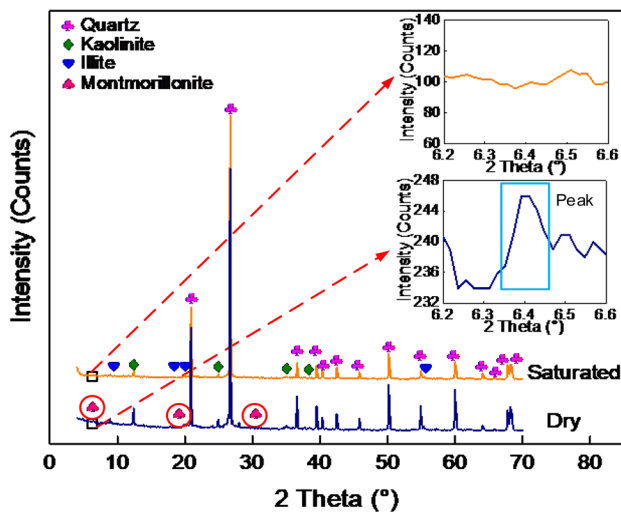
### Mineral composition analysis of rock specimens

The XRD results of the sandstone before and after water intrusion are shown in Fig. 5. According to Fig. 5, the main mineral components of the sandstone specimens are quartz, kaolinite, illite and montmorillonite, among which quartz is dominant, accounting for 91.04% of the total mineral composition, and other clay minerals (kaolinite, illite and montmorillonite) merely account for 8.96%. Kaolinite, illite and montmorillonite account for 44.8%, 34.9% and 20.3% of the clay minerals, respectively. Clay minerals have particularly strong water absorption properties, which will thicken the water film adsorbed by the mineral particles during water intrusion, causing the rock volume to expand (Cherblanc et al. 2016; Colas et al. 2011). Compared with the mineral content in the dry sandstone, the quartz content decreases by 2.64% while the kaolinite and chlorite content increase by 2.27% and 2.19%, respectively. Under normal temperature and pressure, quartz is not affected by water, and its mass would not change. During water intrusion, water molecules enter between kaolinite and illite particles with layered structure and form polarized water molecular layers (Huang and Che 2007). These water molecular layers can continuously absorb water and expand, which increases the masses of the kaolinite and illite. However, there is a seemingly abnormal phenomenon that the three peaks of montmorillonite were not detected after water intrusion (it is clearly shown by enlarging the XRD patterns with the diffraction angle range of 6.2~6.6°), which means the montmorillonite disappeared. This may be an error caused by water evaporation during sample preparation. In short, the content of clay

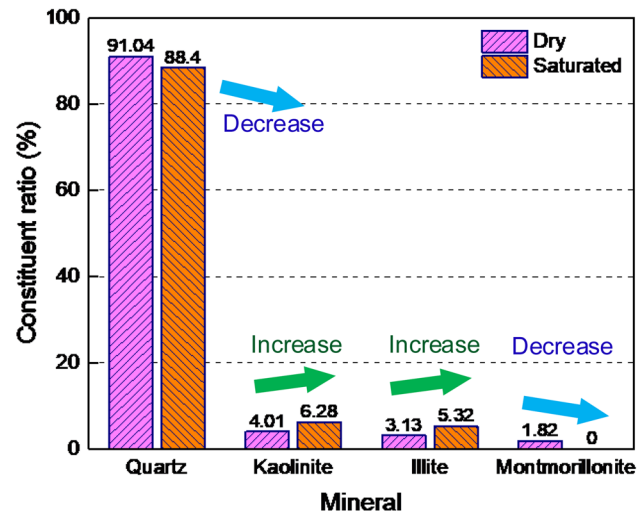
minerals (kaolinite, illite and montmorillonite) is relatively increased under the influence of water.

### Relationship between shear stress and shear displacement of rock joints

Figure 6 illustrates the effects of inclination angle and water content on shear stress–shear displacement curves of the rock joint specimens. According to the failure process, the shear stress–shear displacement curves can be divided into two types. The first type of curves (marked by blue circles in Fig. 6) includes footwall and hanging wall compaction stage, elastic deformation stage, yield and transition stage and post-peak stage (shown in Fig. 7a). At the initial shear stress loading stage, the footwalls and hanging walls of the rock joints are compressed, and the internal primary pores and fractures are compacted and closed. The shear stress–shear displacement curves are concave, and the slopes of these curves increase continuously. In the elastic stage, the shear stress increases approximately linearly with shear displacement. After entering the yield and transition stage, the curves show nonlinear and unstable growth, and the curve slopes gradually decrease. Furthermore, some curves fluctuate as the shear stress gradually increases to the peak. The second type of curves contains five stages (shown in Fig. 7b) with an additional asperity compaction stage (marked by purple circles in Fig. 6) between the elastic stage and the yield and transition stage compared with the first type of curves. In the asperity compaction stage, the curves first exhibit a “convex” shape and then a “concave” shape, and the slope first decreases and then increases accordingly. Combining



a XRD patterns before and after water intrusion



b Change in mineral content

Fig. 5 XRD results of sandstone specimens

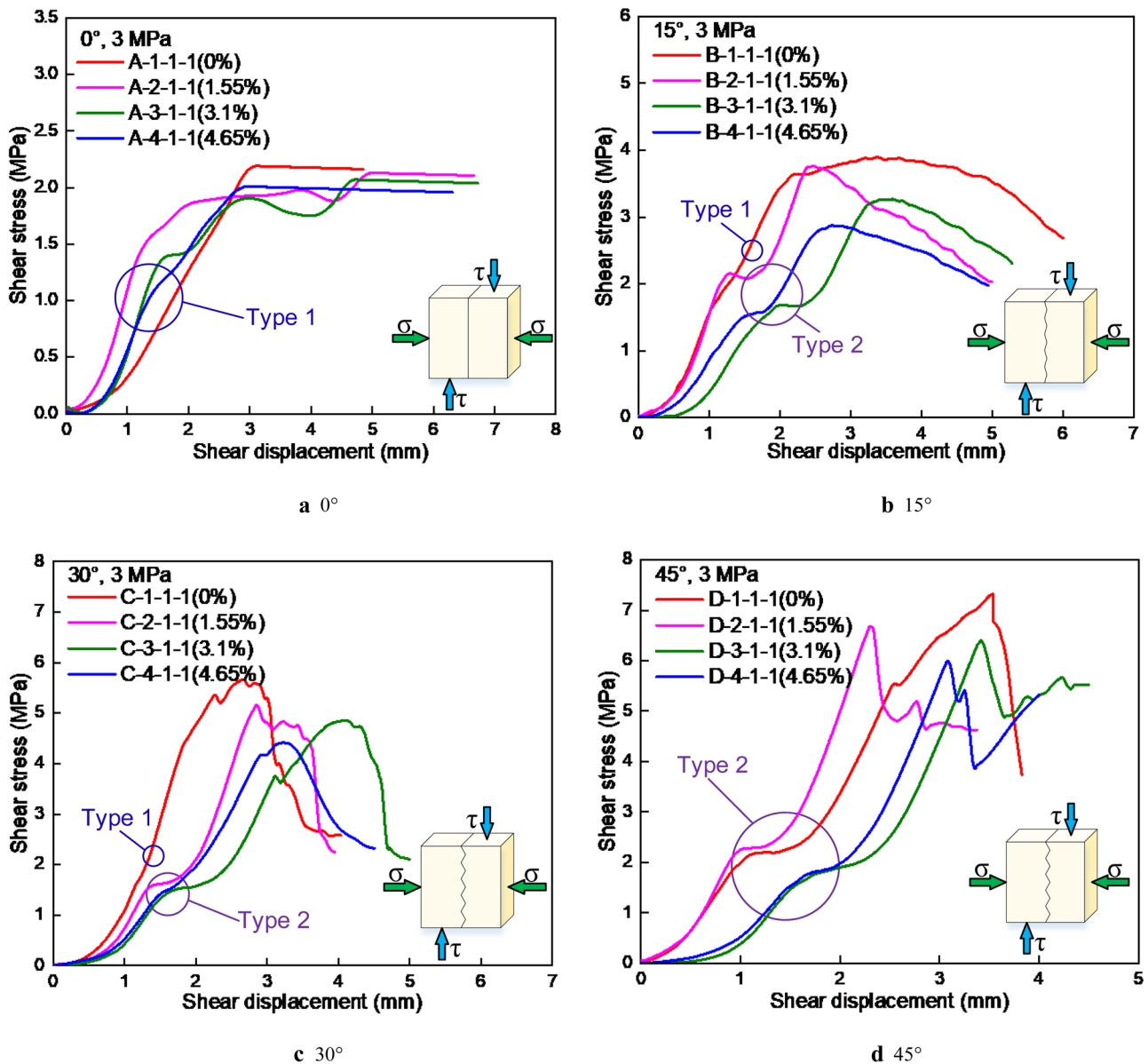


Fig. 6 Relationship between shear stress and shear displacement with a normal stress of 3 MPa and different inclination angles

with the joint damage morphology in Fig. 8 to speculate, this may be because the asperity surface in contact at the joints is damaged, and small force can be added to cause displacement (or deformation) until the joint faces are compacted again.

Whether the shear stress and shear displacement curves include the asperity compaction stage is mainly affected by the inclination angle, but hardly changed by the moisture content or normal stress. With the increasing inclination angle, the number of the first type curves decreases while that of the second type curves increases. When the inclination angle is  $0^\circ$  (Fig. 6a), the corresponding shear

stress–shear displacement curves are all the first type where there are no asperities and no asperity compaction stage. At the inclination angle of  $15^\circ$  (Fig. 6b) and  $30^\circ$  (Fig. 6c), the shear stress–shear displacement curves of specimens B-1-1-1 and C-1-1-1 are of the first type, whereas the others are of the second type. All the shear stress–shear displacement curves with an inclination angle of  $45^\circ$  belong to the second type (Fig. 6d). Under the effect of shear stress, the larger the inclination angle is, the more difficult it is for the asperities of the footwall and hanging wall to slide and the easier it is for joint compression to occur. Thus, the asperity compaction stage is more likely to appear on the

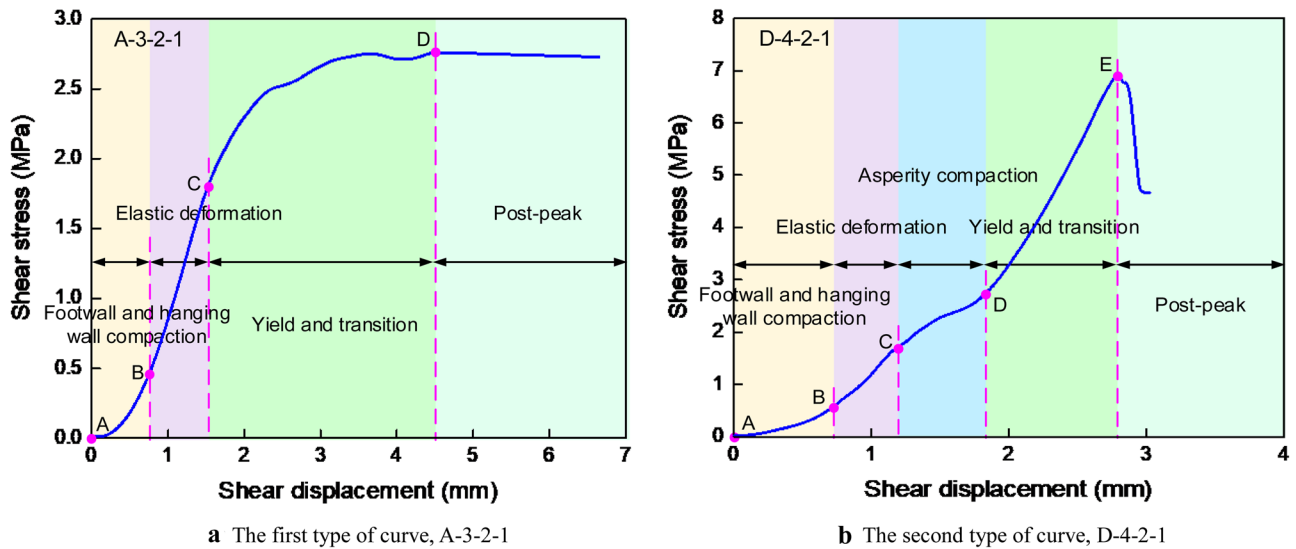


Fig. 7 The two types of shear stress–shear displacement curves of the rock joint specimens

shear stress–shear displacement curves with larger inclination angles.

Inclination angle also plays an important role in the post-peak stage. At 0°, there are no asperities along the rock joints and the failure characteristics are controlled by only the sliding abrasion on the contact areas, thus the post-peak shear stress tends to be stable, reflecting a climbing failure mode. At 15°, the post-peak shear stress decreases gradually, and the absolute values of the corresponding curve slopes are small, which indicates that the asperity tips are compressed and smoothed (“gnawed”) during the sliding abrasion process of rock joint specimens, resulting in the climbing-gnawing combined failure mode. When the inclination angle is 30°, the post-peak shear stress decreases quickly and the curve slopes (absolute values) are large. This is also the climbing-gnawing combined failure mode with weakened climbing failure characteristics and enhanced gnawing failure characteristics compared with 15°. At the inclination angle of 45°, the post-peak shear stress decreases almost vertically, and the asperities of the rock joints are completely sheared with a loud noise, resulting in the gnawing failure mode. When the normal stress increases from 3 to 5 MPa, the absolute values of the slopes of the shear stress–shear displacement curves increase gradually in the post-peak stage, but the increased range is small, and the regularity is not obvious. The increasing normal stress may weaken the climbing failure characteristics and enhance the gnawing failure characteristics.

There is no doubt that the influence of saw-tooth structure inclination angles on the failure behaviours of joints is very great. However, the influence of water cannot be

ignored, because water changes the state of clay minerals through complex physicochemical reactions, which in turn changes the mechanical behaviours of rocks. It is obvious that water reduces the shear strength of the joints (Fig. 9). In Fig. 6a, it is relatively difficult for the water-bearing footwalls and hanging walls to shear slip due to the hindrance of the water-absorbing and expanding clay minerals on the joint surfaces. But where the saw-tooth structure dominates (Fig. 6b–d), water makes shear failure easier. The combination of water and clay minerals increases the plastic deformation capacity of rocks (including joints) and reduces the cohesion and internal friction angle of joints (Fig. 12). Therefore, high moisture content joints deform greatly in the early stage such as footwall and hanging wall compaction stage and elastic deformation stage, and the failure process is also prolonged in the post-peak stage.

### Shear failure characteristics of rock joints

To perform a univariate analysis on the shear failure characteristics of the rock joint specimens, the control variable method is adopted to consider two of the three variables of inclination angle, moisture content and normal stress unchanged. Figure 8a~c show the effect of the inclination angle, normal stress and moisture content, respectively, and Fig. 8d shows the difference between the climbing-gnawing combined failure mode and gnawing failure mode.

According to Fig. 8a, when inclination angle is 0° (no asperities), the specimen only undergoes sliding abrasion, and the white rock dust generated by the friction between



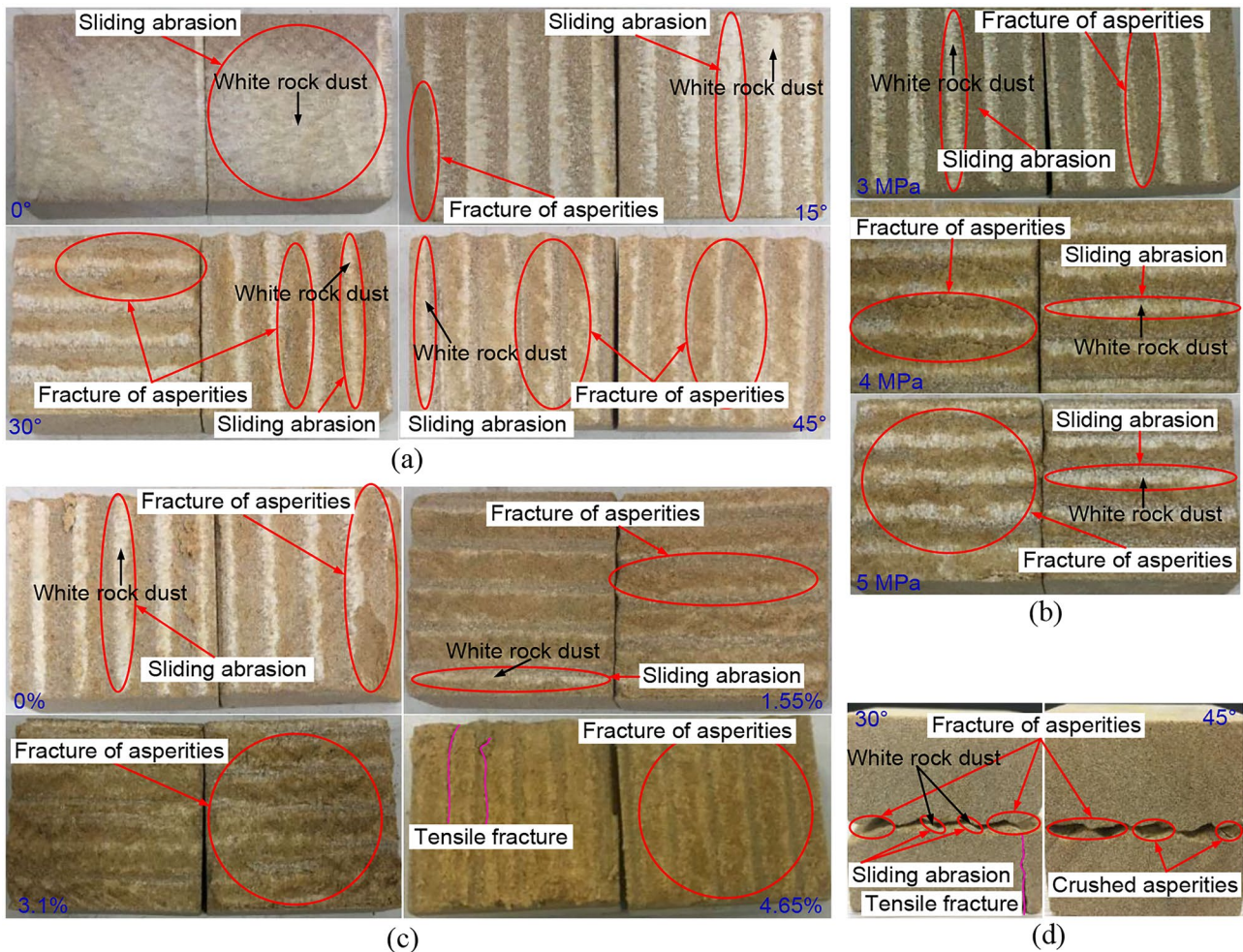


**Fig. 8** Shear failure characteristics of rock joints. **a** Moisture content is 0%; normal stress is 3 MPa. **b** Incline angle is 30°; moisture content is 3.1%. **c** Incline angle is 45°, normal stress is 4 MPa. **d** Moisture content is 1.55%, normal stress is 3 MPa

the footwall and hanging wall covers the whole contact area. At 15°, a certain degree of sliding abrasion occurs on the contact area of the specimen, resulting in white dust, and gnawing failure occurs on some asperity tips. At the inclination angle of 30°, the sliding abrasion degree is reduced while the effect of the shear load on the asperities is enhanced compared with that of 15°. The sliding abrasion degree is very small, and a large number of asperities are cut off at 45°. Figure 8d also shows that sliding abrasion appears in the contact areas of the specimen with the climbing-gnawing combined failure mode while there are almost no signs of abrasion in the gnawing failure mode. These results are consistent with the description in “[Relationship between shear stress and shear displacement of rock joints](#)”.

When normal stress increases from 3 to 5 MPa (Fig. 8b), the sliding abrasion degree of the contact area of the specimen decreases gradually, the amount of white dust

produced by the sliding between the footwall and hanging wall decreases, and the number and range of the gnawed asperities increase. These results indicate that, with increasing normal stress, the climbing failure characteristics are weakened, and the gnawing failure characteristics are enhanced.

Figure 8c shows that, with increasing moisture content, the surface white dust decreases gradually (there is almost no white dust on the contact area of the specimens with a moisture content of 3.1% and 4.65%). Water can lubricate the rock joint surface, which reduces the friction coefficient between the footwall and hanging wall. Compared with specimens with other moisture content, the saturated specimen exhibits tensile cracks and loose rock particles on the joint surfaces. This difference is because water weakens the cementation degree of rock particles and thus reduces the tensile strength of the rock. Under the action of normal stress and shear stress, local tensile stress



is induced in specimens. When the tensile stress reaches the tensile strength, the specimens would show (partial) tensile failure.

### Evolution of the shear mechanical properties of rock joints

#### Shear strength

According to Fig. 9, the shear strength of rock joint specimens is positively correlated with the inclination angle (and normal stress, which is not shown here) and negatively correlated with the moisture content. Under the normal stress condition of 3 MPa, the average shear strength of the rock joint specimens with an inclination angle of 0° decreases from 2.17 to 2.01 MPa from dry to saturated conditions, with a decrease of 7.4%. Similarly, the corresponding decreases of the rock joint specimens with an inclination angle of 15°, 30° and 45° are 14% (from 3.29 to 2.83 MPa), 21.6% (from 5.64 to 4.42 MPa) and 17.7% (from 7.27 to 5.98 MPa), respectively. It can be seen from the slopes of the fitting lines in Fig. 9 that inclination angle increases the slope (absolute value), that is, the impact of water on joint shear strength with large inclination angles is more significant. Note that the correlation coefficient of 0° fitting line is lower (0.74) because smaller values tend to produce larger dispersion. Similarly, with the inclination angle increasing from 0 to 45°, the shear strength of specimens with water content of 0, 1.55%, 3.1% and 4.65% increase by 235%, 218.4%, 212.1% and 197.5%, respectively. This shows that the inclination angle can strengthen the joint strength under the same moisture content.

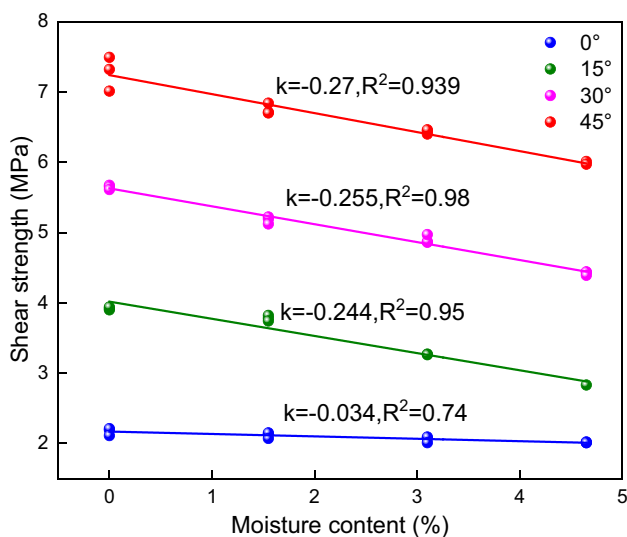


Fig. 9 Shear strength of the rock joint specimens under the normal stress of 3 MPa

#### Shear strength parameters

The Mohr–Coulomb theory, which suggests that the failure mode of rock is mainly shear failure and thus closely related to the normal stress and shear stress (Hudson and Harrison 2000), is widely used in engineering practice. Many experiments and mathematical analyses have proven that the shear strength of rock is determined by the cohesion and internal friction angle. The Mohr–Coulomb model can be used under compression–shear conditions to judge the shear failure of rock or joints simply and quickly (Sun et al. 2006; Yang et al. 2017). The Mohr–Coulomb model is as follows:

$$\tau = c + \sigma \tan \varphi \tag{2}$$

where  $\tau$  is the shear strength, MPa;  $\sigma$  is the normal strength, MPa;  $c$  is the cohesion, MPa; and  $\varphi$  is the internal friction angle, °.

According to Eq. (2), the cohesion and internal friction angle can be obtained, as shown in Fig. 10.

According to Fig. 10, at the inclination angle of 0°, the cohesions of the rock joints with different moisture content are all 0 MPa. When the inclination angle is greater than 0°, the cohesions of the rock joints with different moisture content are greater than 0 MPa. This indicates that the shear strength of the rock joints is completely provided by the internal friction angle in the climbing failure mode. In the climbing–gnawing combined failure mode and the gnawing failure mode, the shear strength of the rock joints is provided by both the cohesion and internal friction angle, and the internal friction angle is controlled by the yield friction and climbing friction of the asperities. With increasing inclination angle, the cohesion and internal friction angle of the rock joints increase linearly. When the inclination angle increases from 0 to 45°, the cohesion of the dry, 1.55% moisture content, 3.1% moisture content and saturated rock joints increases by 4.20 MPa, 3.72 MPa, 3.43 MPa and 3.21 MPa, respectively. The internal friction angle of the dry rock joints increases from 36.3 to 46.1° by 27%. Similarly, the internal friction angle with moisture content of 1.55%, 3.1% and 4.65% increases from 35.8 to 45.6° by 27.4%, from 34.6 to 44.7° by 29.2%, and from 33.4 to 42.9° by 28.4%.

The stress characteristics of a single joint tooth on foot-wall are selected as the study object, as shown in Fig. 11, where  $\theta$  is the inclination angle of the rock joint, °;  $\sigma_n$  is the normal stress, MPa; and  $\tau$  is the shear stress, MPa.  $\sigma_n$  can be decomposed into the compressive stress component  $\sigma_{n1}$  perpendicular to the rock joint and the stress component  $\sigma_{n2}$  along the rock joint;  $\tau$  can be decomposed into the compressive stress component  $\tau_1$  perpendicular to the rock joint and the stress component  $\tau_2$  along the rock joint. The influence of specimen gravity is ignored. The stress perpendicular to the rock joint ( $\sigma_v$ , MPa) is as follows:

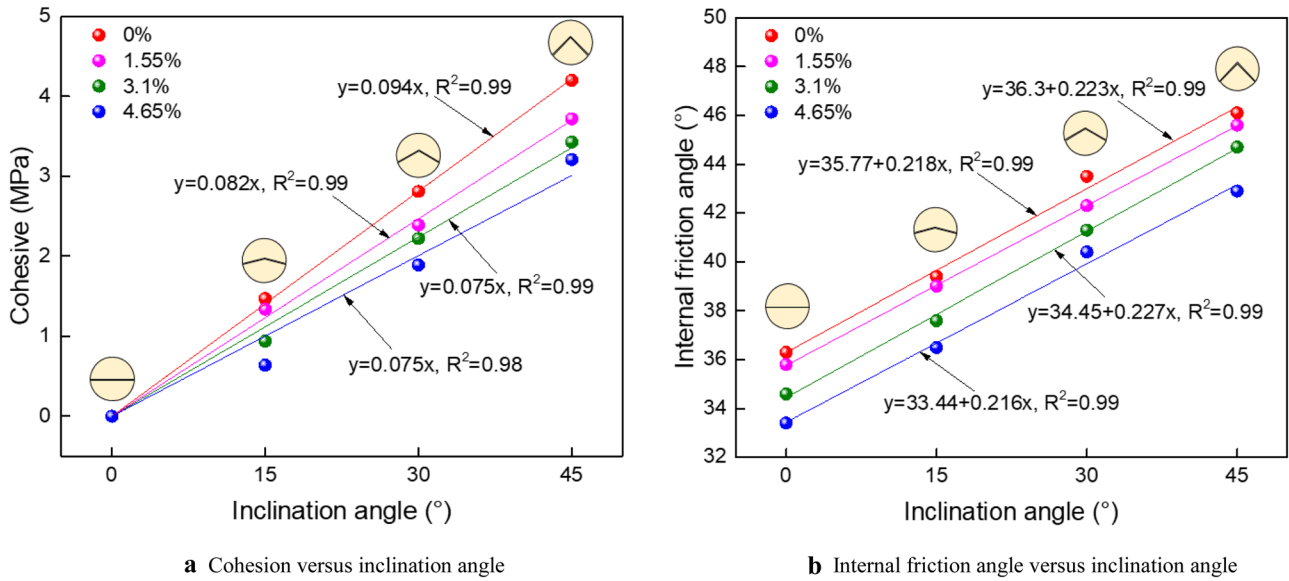


Fig. 10 Effect of the inclination angle on the cohesion and internal friction angle of the rock joints

$$\sigma_v = \sigma_n \cos\theta + \tau \sin\theta \tag{3}$$

The stress along the rock joint ( $\sigma_p$ , MPa) is as follows:

$$\sigma_p = \tau \cos\theta - \sigma_n \sin\theta - \mu(\sigma_n \cos\theta + \tau \sin\theta) \tag{4}$$

where  $\mu$  is the friction coefficient at the contact areas of the rock joint.

According to the definition of  $\sigma_p$ , when  $\sigma_p > 0$ , the rock joint will slide. By assuming  $\sigma_p = 0$ , the minimum shear stress needed for sliding of the rock joint ( $\tau_s$ , MPa) can be obtained:

$$\tau_s = \frac{\sigma_n(\mu + \tan\theta)}{1 - \tan\theta} \tag{5}$$

Because  $\tan\theta$  increases monotonically in  $(-\pi, \pi)$ , with the increase in  $\theta$ ,  $\tau_s$  increases.

According to Eq. (3),  $\sigma_v$  is a function of  $\theta$ . The first derivative of Eq. (3) in terms of  $\theta$  is obtained as follows: By assuming that the first derivative is 0, we obtain the following expression:

$$\sigma'_v = \tau \cos\theta - \sigma_n \sin\theta \tag{6}$$

$$\tau_0 = \sigma_n \cdot \tan\theta \tag{7}$$

By comparing Eqs. (5) and (7), we determine that  $\tau_0$  is less than  $\tau_s$ . When  $\tau$  is greater than  $\tau_0$ , the first derivative of  $\sigma_v$  to  $\theta$  is greater than 0, and  $\sigma_v$  increases monotonically with increasing  $\theta$ .

It can be seen from the above analysis that, with increasing inclination angle, the stress perpendicular to the rock joint and the rock joint friction increases, which causes the cohesion and internal friction angle of the rock joint to increase. Therefore, the shear stress required for the sliding of the rock joint increases, and the sliding of the rock joint becomes more difficult, which means better shear resistance.

The relationship between the cohesion, internal friction angle and moisture content of the rock joints is shown in Fig. 12. The cohesion and internal friction angle generally decrease linearly with moisture content except that the cohesion of 0° inclination angle joint remains the same. From 0 to 4.65% of moisture content, the cohesion of rock joint specimens with inclination angle of 0°, 15°, 30° and 45° decreases by 0, 56.5%, 32.7% and 23.6%, respectively, while the internal friction angle decreases by 8%, 7.4%, 7.1% and 6.9%, respectively. After water intrusion, the water film formed on the rock joint surface reduces the friction coefficient between the footwall and hanging wall. The higher

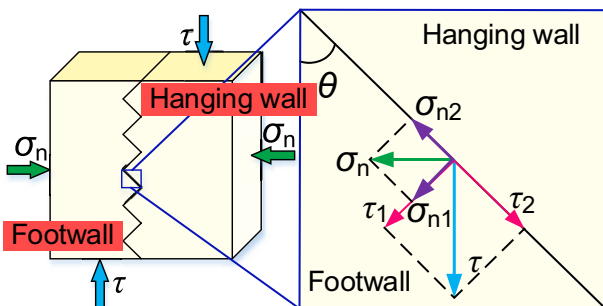


Fig. 11 Force diagram of a rock joint

the moisture content, the lower the friction coefficient. The clay minerals in samples expand with water and compress the surrounding minerals, which changes the microstructure and mechanical parameters of the rock. In addition, water molecules penetrate the rock along the original microcracks, forming water films among the rock particles, weakening the cementation force and reducing the friction coefficient among the particles. Therefore, the cohesion and internal friction angle of the rock joints decrease with water content. Compared with the inclination angle in Fig. 11, water content has less effect on the cohesion and internal friction angle of the rock joints.

### Modified shear strength model

Patton (1966) carried out direct shear tests on regular-tooth gypsum rock joints and proposed the Patton bilinear shear strength formula:

$$\begin{cases} \tau = \sigma \tan(\varphi + i), \sigma \leq \sigma_T \\ \tau = \sigma \tan(\varphi_r + i) + c_r, \sigma > \sigma_T \end{cases} \quad (8)$$

where  $\varphi_r$  is the residual friction angle of the rock joint, °;  $c_r$  is the residual cohesion of the rock joint, MPa; and  $\sigma_T$  is the normal stress of the rock joint at the transition from climbing failure to gnawing failure, MPa.

This formula describes two failure modes: climbing failure under a low normal stress and gnawing failure under a high normal stress. However, in many cases, the failure characteristics of rock joints include both climbing failure and gnawing failure, that is, the climbing-gnawing

combined failure mode. According to “Relationship between shear stress and shear displacement of rock joints”, the degrees of climbing failure and gnawing failure of different rock joints are different. To clarify the physical meaning (i.e., failure modes) of the strength formula of rock joints, based on the test results, Eq. (2) is improved as follows:

$$\tau = \sigma_n \tan[\varphi(\beta, \omega)] + c(\beta, \omega) \quad (9)$$

where  $c(\beta, \omega)$  and  $\varphi(\beta, \omega)$  are the cohesion and internal friction angle of the rock joint, respectively, which are related to the inclination angle and moisture content.

According to Figs. 10 and 12, the cohesion and internal friction angle of rock joints have a linear relationship with the inclination angle and moisture content. Based on the least-square method, the multiple (binary) linear regression analysis method is used to obtain the relationship between the cohesion and inclination angle and the moisture content and the relationship between the internal friction angle and inclination angle and the moisture content. When the inclination angle is 0°, the rock joints show a climbing failure mode at any of the tested moisture content. The cohesion of the rock joints is caused by the gnawing of the asperities. Under the climbing failure mode, the cohesion of the rock joints is 0 MPa. The internal friction angle of the rock joints is controlled by the climbing friction and the yield friction of the asperities. Therefore, when obtaining the relationship between the cohesion and inclination angle and the moisture content of the rock joints, the test data of the rock joints with an inclination angle of 0° are not considered. Accordingly, mathematical models of the binary linear regression analysis

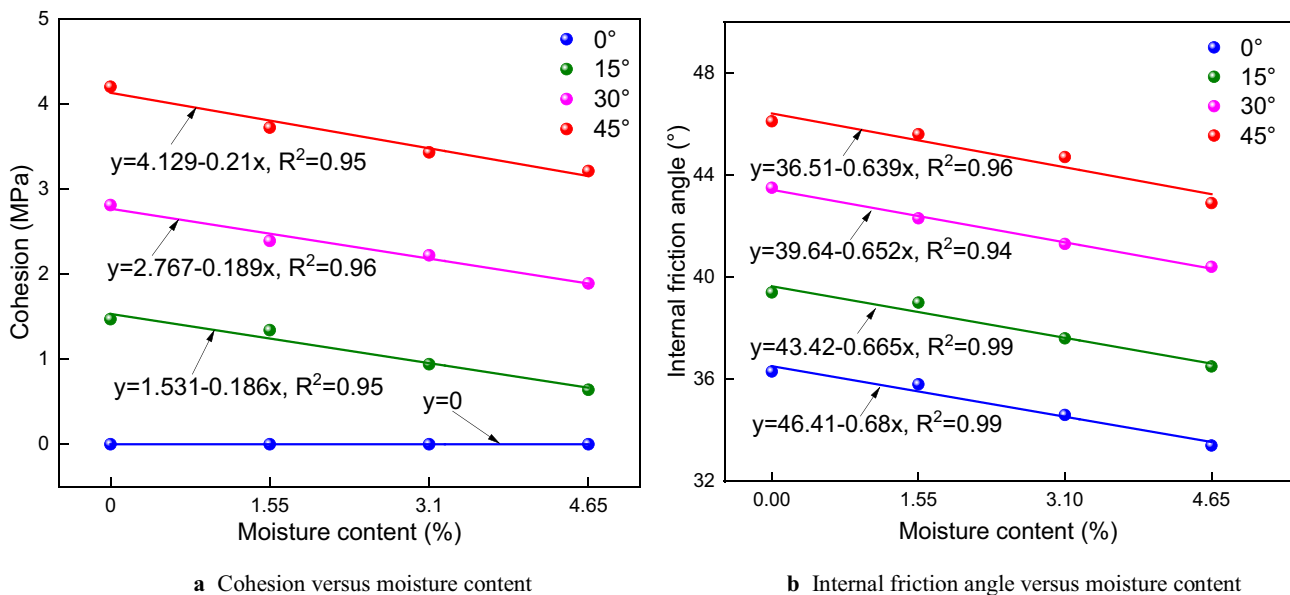


Fig. 12 Effect of the moisture content on the cohesion and internal friction angle of the rock joints

of the cohesion and the internal friction angle of the rock joints are established, which are shown in Eqs. (10) and (11):

$$c = b_0 + b_1\beta_1 + b_2\omega_i \tag{10}$$

where  $i = 1, 2, \dots, 12$  (the four groups of test data excluding the inclination angle of  $0^\circ$ ) and  $b_0, b_1$  and  $b_2$  are all regression parameters.

$$\varphi = k_0 + k_1\beta_j + k_2\omega_j \tag{11}$$

where  $j = 1, 2, \dots, 16$  and  $k_0, k_1$  and  $k_2$  are regression parameters.

The following set of expressions is considered:

$$\begin{cases} C = (c_1 \ c_2 \ \dots \ c_{16})^T, & \phi = (\varphi_1 \ \varphi_2 \ \dots \ \varphi_{16})^T \\ (\beta, \omega)_c = \begin{pmatrix} 1 & \beta_1 & \omega_1 \\ 1 & \beta_2 & \omega_2 \\ \vdots & \vdots & \vdots \\ 1 & \beta_{12} & \omega_{12} \end{pmatrix}, & (\beta, \omega)_\varphi = \begin{pmatrix} 1 & \beta_1 & \omega_1 \\ 1 & \beta_2 & \omega_2 \\ \vdots & \vdots & \vdots \\ 1 & \beta_{16} & \omega_{16} \end{pmatrix} \\ B = (b_0 \ b_1 \ b_2)^T, & K = (k_0 \ k_1 \ k_2)^T \end{cases} \tag{12}$$

where  $C$  is the vector of the cohesion-dependent variable,  $\phi$  is the vector of the internal friction angle-dependent variable,  $(\beta, \omega)_c$  is the matrix of the cohesion-independent variables,  $(\beta, \omega)_\varphi$  is the matrix of cohesion-independent variables,  $B$  is the regression parameter vector of the cohesion and  $K$  is the regression parameter vector of the cohesion. Then, the mathematical models of the cohesion and internal friction angle are as follows:

$$C = (\beta, \omega)B \tag{13}$$

$$\phi = (\beta, \omega)K \tag{14}$$

The results are as follows:

$$B = (b_0 \ b_1 \ b_2)^T = [(\beta, \omega)^T(\beta, \omega)](\beta, \omega)^T C \tag{15}$$

$$K = (k_0 \ k_1 \ k_2)^T = [(\beta, \omega)^T(\beta, \omega)](\beta, \omega)^T \phi \tag{16}$$

According to the least square method, the regression parameter vectors  $B$  and  $K$  are obtained by substituting the experimental data  $c$  and  $\varphi$  into Eqs. (15) and (16), respectively:

$$B = (b_0 \ b_1 \ b_2)^T = (0.27 \ 0.08 \ -0.2)^T \tag{17}$$

$$K = (k_0 \ k_1 \ k_2)^T = (36.52 \ 0.22 \ -0.66)^T \tag{18}$$

The parameters of regression parameter vectors  $B$  and  $K$  are introduced into Eqs. (13) and (14), and the results show that  $c(\beta, \omega)$  and  $\varphi(\beta, \omega)$  of the rock joint specimens are as follows:

$$c(\beta, \omega) = 0.27 + 0.08\beta - 0.2\omega, \ R^2 = 0.99 \tag{19}$$

$$\varphi(\beta, \omega) = 36.52 + 0.22\beta - 0.66\omega, \ R^2 = 0.99 \tag{20}$$

The shear strength formula for rock joints considering the effect of inclination angle and moisture content is obtained by simultaneously solving Eqs. (9), (19) and (20):

$$\tau_p = \sigma_n \tan(36.52 + 0.22\beta - 0.66\omega) + 0.08\beta - 0.2\omega + 0.27 \tag{21}$$

The cohesion in Eq. (21) does not consider the test data of the rock joints with an inclination angle of  $0^\circ$ . Therefore, this equation can only show the relationship between the normal stress and shear strength of rock joints that exhibit the climbing-gnawing combined failure mode and gnawing failure mode but cannot show the relationship in climbing failure mode. To consider the climbing failure mode at the same time, Eq. (21) is improved:

$$\tau_p = \sigma_n \tan(36.52 + 0.22\beta - 0.66\omega) + r(0.08\beta - 0.2\omega + 0.27) \tag{22}$$

where  $r = 0$  when the rock joint exhibits climbing failure and  $r = 1$  when the rock joint exhibits climbing-gnawing combined failure or gnawing failure.

Equation (22) is the modified shear strength formula considering the effect of the inclination angle and moisture content. Since the inclination, normal stress and moisture content all have different degrees of effects on the shear strength and failure characteristics of the rock joints, the critical inclination, moisture content and normal stress of the rock joints that exhibit climbing failure and climbing-gnawing combined failure need to be obtained by constant tests. The theoretical values of the shear strength of rock joints obtained by Eq. (22) are compared with the values obtained experimentally, and the results are in good agreement, as shown in Fig. 13.

### AE count characteristics of the rock joint specimens

The AE count is the number of signal oscillations that exceed the threshold, which is a common AE characterization parameter reflecting the process of internal crack propagation and the damage degree of rock specimens under load. By comparing the response process of the AE count over time with the loading mechanical characteristic curves of the specimens, the internal damage and energy release of the specimens in different loading stages can be more accurately distinguished (Yao et al. 2020; Zhang et al. 2019). The stress-AE count-cumulative AE count-time curves of these rock joint specimens are shown in Fig. 14. Among them, A-1-1-1, B-1-1-1, C-1-1-1 and D-1-1-1 are used to analyse the influence of the inclination angle on the AE count characteristics of the rock joint specimens: D-1-1-1,



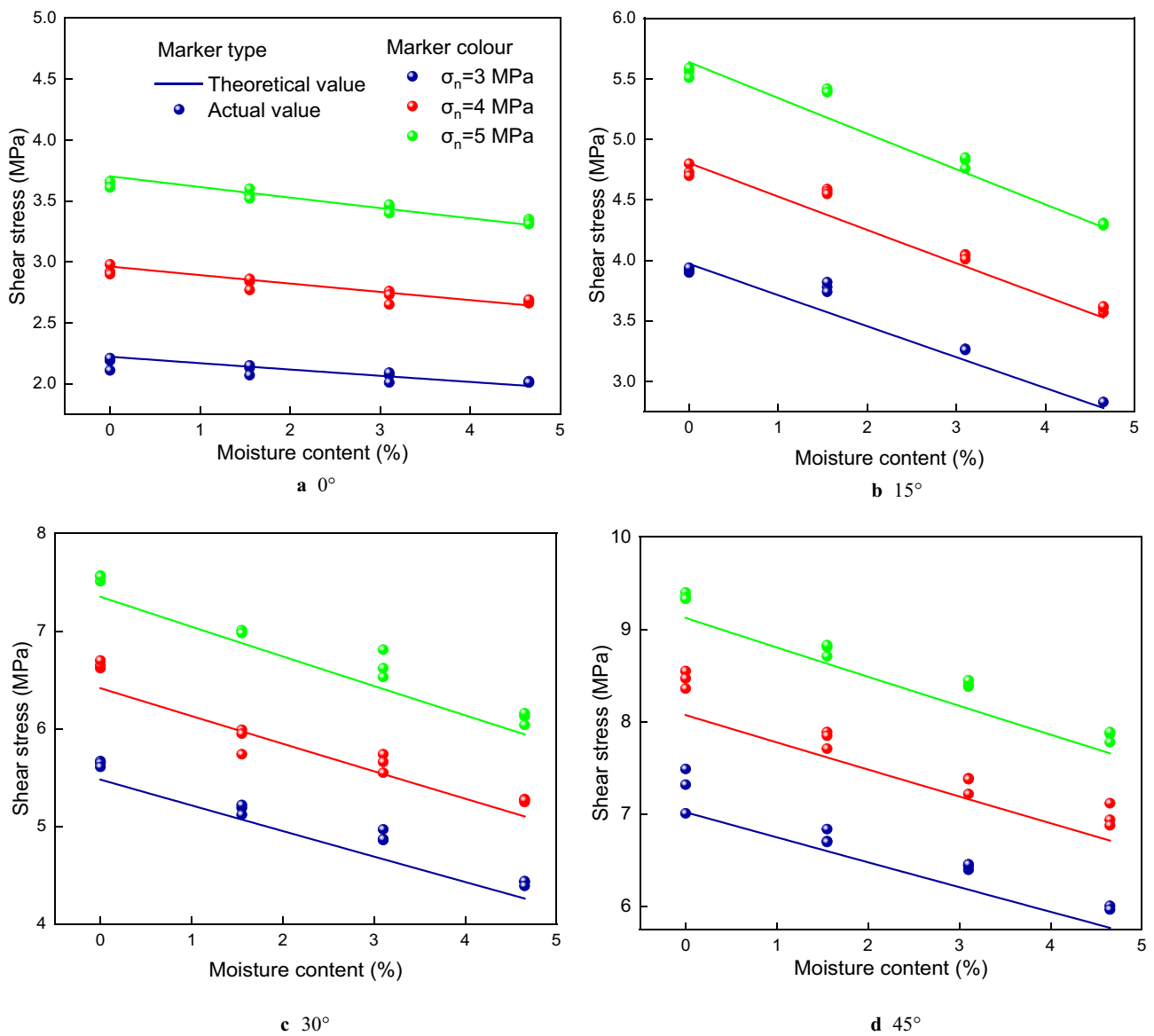


**Fig. 13** Comparison of the theoretical and measured shear strengths of the rock joints with different inclination angles. (Marker type and colour only shown in a)

D-2-1-1, D-3-1-1 and D-4-1-1 are used to study the effect of the moisture content.

According to Fig. 14, during the loading failure process of the rock joint specimens, the AE counts of A-1-1-1 in different stages change insignificantly, and the cumulative AE count curve increases linearly. This is because the inclination angle of A-1-1-1 is  $0^\circ$ , and only sliding abrasion occurs with small AE counts under the action of load. Except for A-1-1-1, when the shear stress approaches the shear strength of the specimens, the AE counts are the most obvious because the internal change is the most violent and macroscale failure of the specimens occurs. The AE count-time curves and cumulative AE count-time curves of specimens with

different rock joints are similar to the corresponding shear stress-time curves, which increase with time and exhibit stages. During the footwall and hanging wall compaction stage, the AE activity is very low, and the internal pores are gradually compacted and closed, releasing a small amount of energy. With increasing load, the specimens gradually enter the elastic deformation stage, the AE counts are significantly greater than those at the footwall and hanging wall compaction stage, and the cumulative AE count-time curves increase linearly. During the asperity compaction stage (D-1-1-1, D-2-1-1, D-3-1-1 and D-4-1-1), the variations in the AE count and cumulative count with time are similar to that in the elastic stage. When the specimens enter the

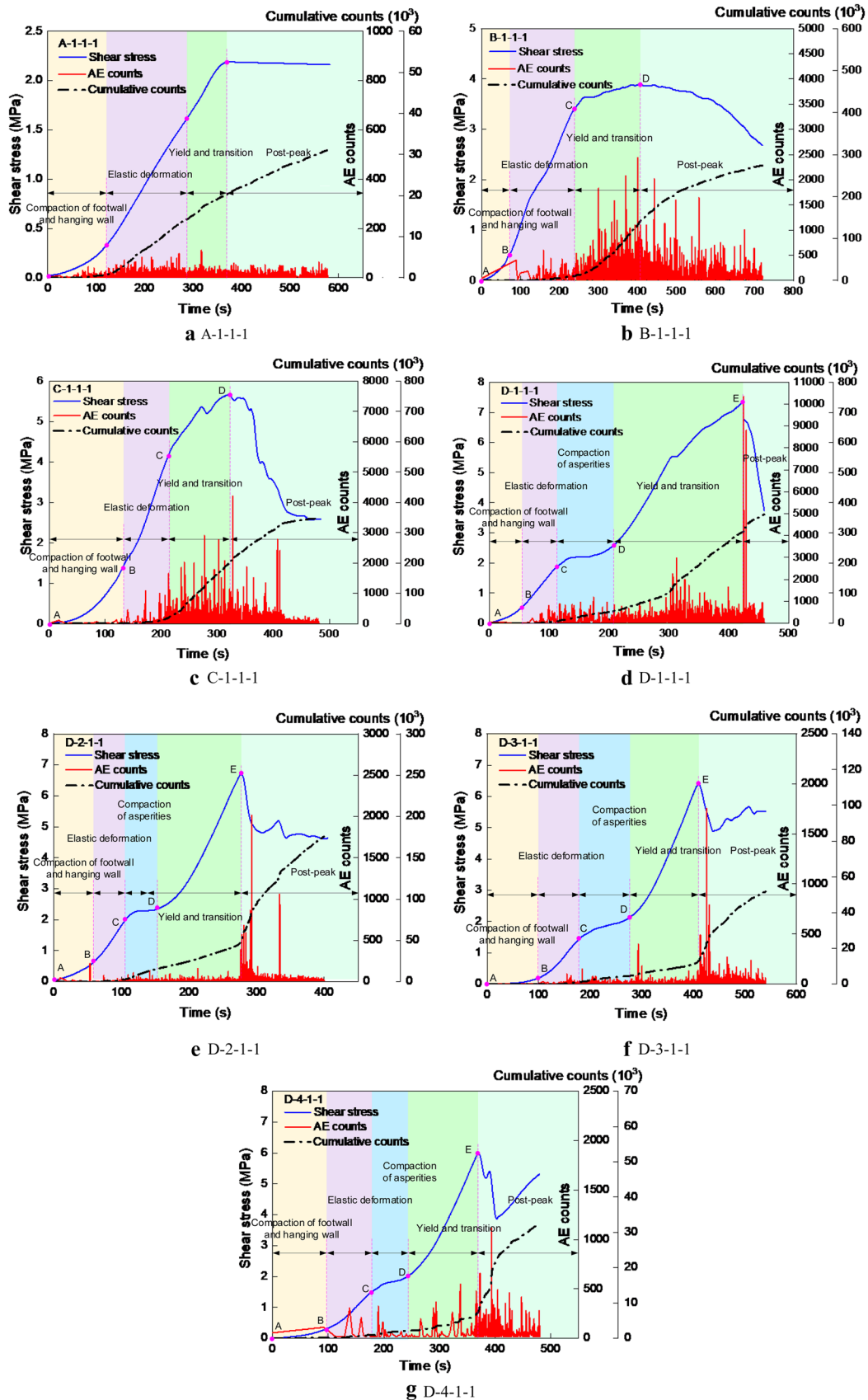


Fig. 14 AE count characteristics with different inclination angles and moisture content

yield and transition stage, several AE counts are significantly higher than the general results, and the slopes of the cumulative AE count-time curves increase, which indicates that the damage process of the internal structure of the specimens is violent. When the shear stresses reach their peak values, the rock joints are damaged, the AE counts peak and the cumulative AE count-time curves increase sharply, indicating that a considerable number of AE signals and amount of energy are released at this time. During the post-peak stage, the AE counts decrease, and the slopes of the cumulative AE count-time curves show decrease trend. The AE signals in this stage are generated by the normal stress crushing the gnawed asperities and the sliding friction between the footwall and hanging wall.

The maximum AE counts of A-1-1-1, B-1-1-1, C-1-1-1 and D-1-1-1 are 111, 2436, 4206 and 10,343, respectively. This means the maximum AE count gradually increases with inclination angle. The reason is that the weakened climbing failure characteristics and the strengthened gnawing failure characteristics cause the damage degree of the asperities to increase with inclination angle, thus the strengths and magnitudes of the AE signals released during the failure increase.

Comparing D-1-1-1, D-2-1-1, D-3-1-1 and D-4-1-1, the AE count and frequency of the specimens decrease gradually with moisture content. From dry to saturated states, the maximum AE counts decrease from 10,343 to 1120 by 89.2%. This indicates that water has an inhibitory effect on the AE signals of rock joints, and the higher the moisture content is, the more obvious this inhibitory effect. Water weakens the internal structure and stress of the specimens, decreases the friction coefficient between the footwall and hanging wall of the rock joints and among the particles in the asperities, and thus reduces the damage activity and the energy required for instability. At the macroscale, the maximum (cumulative) AE counts are reduced due to the effect of water.

## Conclusions

In this work, the water absorption characteristics and mineral composition of the sandstone specimens were tested, the direct shear tests of saw-tooth rock joint specimens with different inclination angles, normal stresses and moisture content were carried out, and the AE signals during the tests were monitored. According to the test results and theoretical analysis, the following conclusions can be drawn.

(1) The variation of water content with time can be divided into three stages: rapidly rising stage (0~384 min), slowly rising stage (384~4000 min) and stable stage (4000 min~). The main minerals of sandstone include quartz, kaolinite, illite and montmorillonite. After water

intrusion, the content of quartz decreases, while kaolinite and illite increase, except that montmorillonite is a little controversial.

(2) There are two types of shear stress-shear displacement curves. The first type includes the footwall and hanging wall compaction, elastic deformation, yield and transition and post-peak stages. The second type contains the footwall and hanging wall compaction, elastic deformation, asperity compaction, yield and transition and post-peak stages. The inclination angle has the greatest effect on the shear failure modes of rock joint specimens, followed by the normal stress, and the moisture content has the least effect. At the inclination angle of 0°, the failure mode is climbing. At 15° or 30°, the failure mode is climbing-gnawing combined. At 45°, the failure mode is gnawing.

(3) The shear strength is positively correlated with the inclination angle and normal stress and negatively correlated with the moisture content. With increasing inclination angle, the cohesion and internal friction angle increase linearly. With increasing moisture content, the cohesion and internal friction angle decrease linearly. According to the test data, based on the Mohr-Coulomb model, the shear strength formula of rock joints considering the effect of inclination angle and moisture content is established by using the binary linear regression analysis method.

(4) Except for the specimens with an inclination angle of 0°, the AE count and cumulative count curves of the other specimens correlate well with the stress curves in the test process. The combination of these three curves can better analyse the internal damage activity, crack propagation and structure failure of the specimens in each stage of the loading process. With increasing inclination angle, the maximum AE count gradually increases; with increasing moisture content, the maximum AE count gradually decreases.

**Funding** This work was supported by the National Natural Science Foundation of China (51674248 and 51874283).

## References

- Bahaaddini M (2017) Effect of boundary condition on the shear behaviour of rock joints in the direct shear test. *Rock Mech Rock Eng* 50(5):1141–1155
- Barton NR, Choubey V (1977) The shear strength of rock joints in theory and practice. *Rock Mech* 10(1):1–54
- Clarkson L, Williams D (2021) An overview of conventional tailings dam geotechnical failure mechanisms. *Min Metallur Explor* 38:1305–1328
- Cabrera M, Senent S, Olalla C, Jimenez R (2015) Sliding stability analysis of gravity dam founded on rock mass with impersistent joint set. *Can Geotech J* 52(11):1668–1684

- Cherblanc F, Berthouneau J, Bromblet P, Huon V (2016) Influence of water content on the mechanical behaviour of limestone: role of the clay minerals content. *Rock Mech Rock Eng* 49(6):2033–2042
- Colas E, Mertz JD, Thomachot-Schneider C, Barbin V, Rassineux F (2011) Influence of the clay coating properties on the dilation behavior of sandstones. *Appl Clay Sci* 52(3):245–252
- Deb D, Das KC (2014) A new doubly enriched finite element for modelling grouted bolt crossed by rock joint. *Int J Rock Mech Min Sci* 70:47–58
- Gu DM, Huang D, Yang WD, Zhu JL, Fu GY (2017) Understanding the triggering mechanism and possible kinematic evolution of a reactivated landslide in the three gorges reservoir. *Landslides* 14(6):2073–2087
- Hudson JA, Harrison JP (2000) *Engineering rock mechanics—an introduction to the principles*. Elsevier, New York, USA
- Huang HW, Che P (2007) Research on micro-mechanism of softening and argillitization of mudstone. *J Tongji Univ (nat Sci)* 7:866–870 (in Chinese)
- Indraratna B, Haque A (1997) Experimental study of shear behavior of rock joints under constant normal stiffness conditions. *Int J Rock Mech Min Sci* 34(3–4):141
- Jia P, Zhu WC (2012) Dynamic-static coupling analysis on rockburst mechanism in jointed rock mass. *J Central South Univ* 19(11):3285–3290
- Kalachev VA, Zaitsev DV, Kochanov AN, Kostandov Y, Panfilov PE (2018) Effect of water on fracture of rocks under diametral compression. In *IOP Conference Series: Earth and Environmental Science* (Vol. 134, No. 1, p. 012023). IOP Publishing
- Kostic S (2017) Analytical models for estimation of slope stability in homogeneous intact and jointed rock masses with a single joint. *Int J Geomech* 17(10):0401708910
- Kou MM, Liu XR, Tang SD, Wang YT (2019) Experimental study of the prepeak cyclic shear mechanical behaviors of artificial rock joints with multiscale asperities. *Soil Dyn Earthq Eng* 120:58–74
- Kulatilake P, Liang J, Gao H (2001) Experimental and numerical simulations of jointed rock block strength under uniaxial loading. *J Eng Mech-Asce* 127(12):1240–1247
- Ladanyi B, Archambault G (1970) Simulation of shear behavior of a jointed rock mass. In *The 11th US Symposium on Rock Mechanics (USRMS)*, Berkeley. OnePetro
- Lee HS, Park YJ, Cho TF, You KH (2001) Influence of asperity degradation on the mechanical behavior of rough rock joints under cyclic shear loading. *Int J Rock Mech Min Sci* 38(7):967–980
- Li KH, Cao P, Zhang K, Zhong YF (2015) Macro and meso characteristics evolution on shear behavior of rock joints. *J Central South Univ* 22(8):3087–3096
- Liu MX, Liu EL (2017) Dynamic mechanical properties of artificial jointed rock samples subjected to cyclic triaxial loading. *Int J Rock Mech Min Sci* 98:54–66
- Lockner D (1993) The role of acoustic emission in the study of rock fracture. *Intern J Rock Mech Min Sci Geomech Abs* 30(7):883–899
- Maruvanchery V, Kim E (2019) Effects of water on rock fracture properties: studies of mode I fracture toughness, crack propagation velocity, and consumed energy in calcite-cemented sandstone. *Geomech Eng* 17(1):57–67
- Marc O, Stumpf A, Malet JP, Gosset M, Uchida T, Chiang SH (2018) Initial insights from a global database of rainfall-induced landslide inventories: the weak influence of slope and strong influence of total storm rainfall. *Earth Surf Dyn* 6(4):903–922
- Meng FZ, Zhou H, Wang ZQ, Zhang LM, Kong L, Li SJ et al (2016) Experimental study on the prediction of rockburst hazards induced by dynamic structural plane shearing in deeply buried hard rock tunnels. *Int J Rock Mech Min Sci* 86:210–223
- Patton FD (1966) Multiple modes of shear failure in rock. In *1st ISRM Congress. Intern Soc Rock Mech Rock Eng*
- Plesha ME (1987) Constitutive models for rock discontinuities with dilatancy and degradation. *Int J Numer Anal Meth Geomech* 11(4):345–362
- Salimian MH, Baghbanan A, Hashemolhosseini H, Dehghanipoodeh M, Norouzi S (2017) Effect of grouting on shear behavior of rock joint. *Intern J Rock Mech Min Sci* 98:159–166
- Saeb S, Amadei B (1992) Modelling rock joints under shear and normal loading. *Intern J Rock Mech Min Sci Geomech Abs* 29(3):267–278
- Sun DA, Yao YP, Matsuoka H (2006) Modification of critical state models by Mohr-Coulomb criterion. *Mech Res Commun* 33(2):217–232
- Tada H, Ishizuka Y, Horii H, Uchita Y, Kashiwayanagi M (2002) Kimata H (2002) Stability evaluation method of dam foundation during earthquake in consideration of rock joints. *Japan Soci Civil Eng* 715:201–213
- Tang CJ, Yao QL, Li ZY, Zhang Y, Ju MH (2019a) Experimental study of shear failure and crack propagation in water-bearing coal samples. *Energy Sci Eng* 7(5):2193–2204
- Tang CJ, Yao QL, Xu Q, Shan CH, Xu JM, Han H, Guo HT (2021) Mechanical failure modes and fractal characteristics of coal samples under repeated drying–saturation conditions *Nat Resour Res* 1–18. <https://doi.org/10.1007/s11053-021-09905-6>
- Tang ZC, Zhang QZ, Peng J, Jiao YY (2019b) Experimental study on the water-weakening shear behaviors of sandstone joints collected from the middle region of Yunnan province, P.R. China. *Eng Geol* 258:105161
- Wang F, Cao P, Cao RH, Xiong XG, Ji H (2019) The influence of temperature and time on water-rock interactions based on the morphology of rock joint surfaces. *Bull Eng Geol Env* 78(5):3385–3394
- Yang H, Duan HF, Zhu JB (2019) Ultrasonic P-wave propagation through water-filled rock joint: an experimental investigation. *J Appl Geophys* 169:1–14
- Yang SQ, Tian WL, Ranjith PG (2017) Experimental investigation on deformation failure characteristics of crystalline marble under triaxial cyclic loading. *Rock Mech Rock Eng* 50(11):2871–2889
- Yao QL, Chen T, Ju MH, Liang S, Liu YP, Li XH (2016) Effects of water intrusion on mechanical properties of and crack propagation in coal. *Rock Mech Rock Eng* 49(12):4699–4709
- Yao QL, Tang CJ, Xia Z, Liu XL, Zhu L, Chong ZH, Hui XD (2020) Mechanisms of failure in coal samples from underground water reservoir. *Eng Geol* 267:105494
- Zhang Y, Feng XT, Yang CX, Zhang XW, Sharifzadeh M, Wang ZF (2019) Fracturing evolution analysis of beishan granite under true triaxial compression based on acoustic emission and strain energy. *Int J Rock Mech Min Sci* 117:150–161
- Zhou H, Meng FZ, Zhang CQ, Hu DW, Lu JJ, Xu RC (2016) Investigation of the acoustic emission characteristics of artificial saw-tooth joints under shearing condition. *Acta Geotech* 11(4):925–939
- Zhou JR, Wei X, Yang TH, Zhu WC, Li LC, Zhang PH (2018) Damage analysis of rock mass coupling joints, water and microseismicity. *Tunn Undergr Space Technol* 71:366–381